# Experimental Studies on Gas Explosions by Different Obstacles in a Partially Confined Region

**Y.S. Lee[1], D.J. Park[2], A.R. Green[2] and N.Y. Park[1]**

[1]*Dept. of Safety Engineering, Seoul National University of Technology, Seoul 139-743, Korea*
[2]*School of Safety Science, The University of New South Wales, NSW 2052, Australia*

## Abstract

Experimental investigations were performed to assess the effects of different obstacle obstructions in a partially confined rig, 235 mm in height, with a 1000 × 950 $mm^2$ cross section and with large top-venting of area 1000 × 320 $mm^2$. Three different single and multiple obstacles with cylindrical, triangular and square cross sections covering blockage ratios ranging from 5 to 30 % were used. High speed video was used to record the flame paths and lengths. These were correlated with pressure measurements. The square obstructions with the lowest volume yielded the lowest overpressures while the highest overpressures were obtained with the cylindrical obstructions. The explosion pressure was found to decrease with increasing blockage ratio and with the single obstacles rather than the multiple ones due to the formation of lower volumes of unreacted mixture.

**Keywords:** Explosion pressure; Flame propagation; Obstacles

## 1. Introduction

Past accidents have demonstrated that the most severe threat to some industries such as chemical and petrochemical industries is the hazard of gas explosions, which have been the predominant causes of high damage accidents in these industries [10]. 42 % of the largest insurer losses between 1957-1986 were due to gas explosions [2], and the property losses due to the explosions as reported by Lenori and Davenport [11] accounted for 37% in excess of $ 50 m. As presented by Khan and Abbasi [9], although infrequent, the highest fatalities per major accidents were related to explosions.

Thus, gas explosions have a considerable implication on the safety in terms of potential loss of life, asset and business interruption risks. In particular, explosions occurring in confined and partially-confined regions are of special concern due to the potential for domino effects and more serious consequences [4]. Therefore, prediction of overpressures has been of great interest and a knowledge of the likely overpressure has been needed for the design of equipment, safety cases and emergency planning [1]. In order to obtain an acceptable level of safety in design and operation levels of such installations, the

*Corresponding Author- Tel.*: +61-2-9385-5002;
*Fax*: +61-2-9385-6190
*E-mail address*: pdj70@hanmail.net

risk assessment of gas explosions is an important process.

For such assessments, predictive tools that accurately predict gas explosions are needed. The tools should be validated against sufficient experimental data before its can become a useful tool [5]. A rapidly growing number of CFD explosion codes such as EXSIM, FLACS, AutoReaGas, COBRA, etc. are being used in explosion assessments [16].

These codes give the better potential of providing high accuracy and more detailed information like flow speed, temperature, concentration, pressure, flame speed, etc. that are useful for designing against gas explosion. However, the tools currently available have only been tested against very limited experimental data. The accuracy of a CFD simulation is limited by the accuracy of the numerical model and the underlying physical sub-models such as combustion & turbulence [17].

Experimental studies are also required to further understand the physical processes, and the data gained is crucial for the validation of physical submodels which may be used to improve adequate predictive tools [3].

Over the last decade, the majority of both large- and small- scale experiments have been performed to investigate the interaction between the propagating flame and obstacles inside various geometries with large L/D (length to diameter ratio) such as in vessels and cylindrical tubes. The large scale studies with L/D of approximately 4 by Moen et al. [13,14] and Hjertager et al. [6] revealed that the existence of obstacles had a profound effect on the flame propagation due to the generation of turbulence. The flame speed was found to depend on the size of obstacles and fuel/air mixtures.

The experiments of Urtiew et al. [18] in partially confined geometries with L/D ratios of 6 and the investigations of the influence of a single obstacle such as an orifice, circular plate, or wire gird on flame propagation in cylindrical tube with an L/D between 3 to 5 by Starke and Roth [19] indicated that obstacles can increase the speed of flame propagation and the effects of an obstacle depend on its position in the rig. The effects of a single baffle on flame speeds and rates of pressure rise with varying blockage ratio (20-80%) in long tubes as large L/D of 22 by Phylaktou & Andrews [15] and the studies of explosion overpressures and imaged flame front location in a vessel where baffle plates were placed at various distances along the wall of the enclosure with L/D ratios of 4 by Pritchard et al. [17] have shown that the flame speed and rate of pressure rise were enhanced downstream of the baffle, and the relative effect of the baffle increased with increasing blockage ratio.

Studies by Fairweather et al. [3] in a cylindrical tube with an L/D of 2-3 where obstruction rings were placed at various axial locations on the wall of the cylinder have shown that significant overpressures were generated in the later stages of explosions because of rapid turbulent combustion in the shear layers and recirculation zones induced by the obstacles.

Recently studies by Masri et al. [12], and Ibrahim and Masri [8] to investigate the interaction between the propagating flame and solid obstacles which have various blockage ratio (8.7-78.3%) mounted inside a cylindrical vessel with L/D of 2.8 have shown that the cylindrical obstruction resulted in the lowest overpressures due to lower flame acceleration behind the obstacle while plates or wall type obstructions caused the highest overpressures because of higher flame acceleration. The acceleration was associated with the volume of trapped unburnt mixture behind obstacle wake. Also, studies of Ibrahim et al. [7] indicated that flame deceleration was observed due to the faster reduction in the volume of the unburnt mixture inside the chamber towards the chamber exit and the flame surface area. The

amount of the unburnt mixture behind the obstacle wake was dependent on the rate of change of the flame front length.

All of the above-mentioned experiments on the interaction of the flame propagation and obstacles have been done in large L/D enclosures. Their results revealed that there is a strong interaction between the turbulence level formed behind the obstacle and the resulting peak pressure, and the turbulent flame and turbulence interaction trapped behind the obstruction greatly enhance the speed of flame propagation and hence increase the rate of pressure rise. However, in practical enclosures with small L/D ratios and having a large venting area, the interactions between the flame and various obstacles compared with large L/D enclosures are quiet likely to be different.

The present work was aimed at providing experimental data necessary for the development of a physical sub-model of combustion for CFD (Computation Fluid Dynamics) and investigating the underlying mechanisms of the phenomena observed in terms of flame behaviour, flame height and width for the propagating flame front, overpressure and the rate of pressure rise and impulse through different single and multiple obstacles in a partially confined enclosure with small L/D ratios and large vent area.

## 2. Experimental

As shown in Fig. 1, a schematic diagram of the experimental set-up, the rig used consisted of an explosion chamber, 235 mm in height, 1000 × 950 $mm^2$ in cross section and with large top-venting of area 1000 × 320 $mm^2$ giving a total volume of 223 liters of explosive mixture and a vent to volume ratio of 0.8695. The rig was made of 20 mm thick transparent chemiglass restrained by bolted flanges and strong adhesives. Flammable gas (99.95 % $CH_4$ by vol.) entered the box through the valve placed in the bottom of the side wall of the chamber. The fuel volume flow rates were monitored using a calibrated gas flow control system (TEI, Model GFC 521).

Before gas filling, the large rectangular vent of area 1000 × 320 $mm^2$ was covered with thin plastic film (household plastic wrap). The film was sealed on a layer of blue tak lined around the vent. Air within the chamber during the filling sequence was continuously withdrawn via the open sample ports positioned at three different locations.

The fuel/air mixture was circulated through the explosion chamber using a recirculation pump for several minutes to ensure a completely homogeneous mixture and then allowed to settle for several

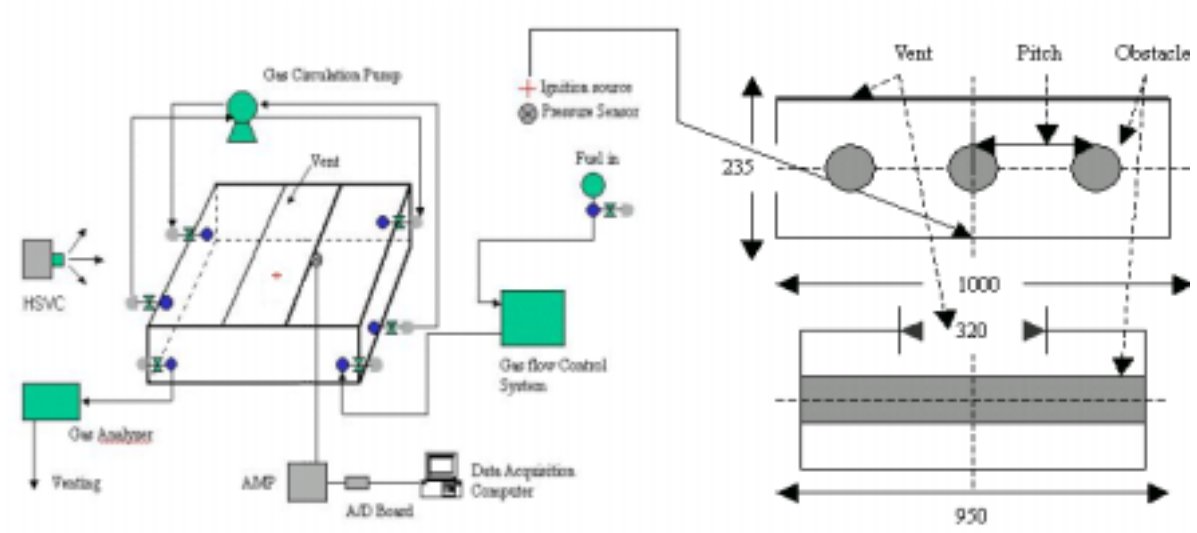


Figure 1. Schematic diagram of the experimental arrangements and rig.

minutes before ignition. The fuel concentration was monitored by an infrared gas analyzer (GDA, Model LMSx) with an accuracy of ± 0.3%. The calibration of the apparatus was periodically checked by injecting calibration gases of known composition into the measurement system.

The flammable mixture within the chamber was ignited by a 15.5 KV electric spark positioned near the centre of the bottom wall, when the contact switch was closed. The flame images were photographed with a high speed video camera (KODAK Motion corder Analyzer, SR-ULTRA-C) operating at the rate of 500 frame/s, providing a temporal resolution of 2 ms. The pressure was recorded using a dynamic pressure transducer with a range of 0-2.5 bar (KISTLER type 701 A). Signals from the pressure transducer were logged on a 16 bit A/D converter sampling at 2 kHz, and a channel charge amplifier (KISTLER type 5019 B) and data acquisition computer were used to record pressure data.

As shown in Table 1, different single and multiples obstacles such as circular cylinder, square and triangular bars with blockage ratios ranging from 5% to 30% were mounted inside the chamber and centred 117.5 mm from the bottom of the chamber. The estimation of blockage ratio is an area percentage defined as the largest cross-sectional area blocked by positioning the obstruction in the explosion chamber divided by the cross-sectional area of the explosion chamber which is (1000×950) $mm^2$ [12].

In all the experiments reported, the methane concentration in air was 10±0.2% a slightly rich mixture of methane and air. Each test was repeated at least five times in order to ensure reproducibility and average values were used, and the reproducibility between all tests was found to be reasonable: the error was ±5% in time and ±5% in pressure.

## 3. Results and discussion

### 3.1 Effects on flame behaviour

Fig. 2 shows a sequence of high-speed images of flame propagation during the course of the explosions with single and multiple obstacles of circular, triangular and square cross-sections, respectively. The time shown represents elapsed time after ignition and subsequent flame images are at 30 ms intervals.

The flame in the early stages of flame propagation for all obstacles used is an expanding hemisphere from the bottom of the chamber. At around 24-30 ms after

Table 1. The different single and multiple obstacles used in the explosion chamber

| | Obstacle shapes | Symbol | Dimensions (mm) | Blockage ratio (%) |
|---|---|---|---|---|
| Single obstacles | Cylinder, side-on | SC1 | Length 950 × Diameter 50 | 5 |
| | | SC2 | Length 950 × Diameter 100 | 10 |
| | Square Bar, face-on | SS1 | Length 950 × Side 50 | 5 |
| | | SS2 | Length 950 × Side 100 | 10 |
| | Triangular Bar, side-on | ST1 | Length 950 × Equal sides 50 | 5 |
| | | ST2 | Length 950 × Equal sides 100 | 10 |
| Multiple obstacles | Cylinder, side-on | MC1 | Three sequential SC1, Pitch = 5D | 15 |
| | | MC2 | Three sequential SC2, Pitch = 2.5D | 30 |
| | Square Bars, face-on | MS1 | Three sequential SS1, Pitch = 5D | 15 |
| | | MS2 | Three sequential SS2, Pitch = 2.5D | 30 |
| | Triangular Bars, side-on | MT1 | Three sequential ST1, Pitch = 5D | 15 |
| | | MT2 | Three sequential ST2, Pitch = 2.5D | 30 |

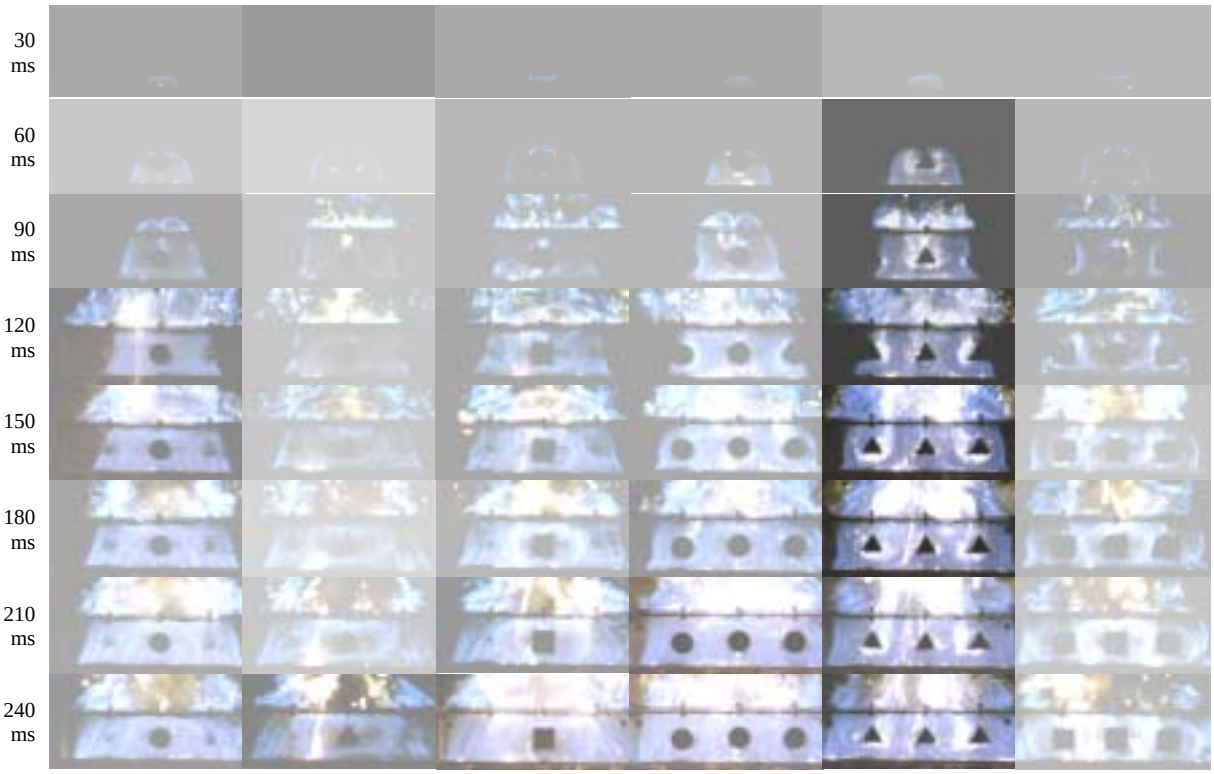


Fig. 2. A sequence of high speed images of flame propagation during the course of explosions with single and multiple cross section obstacles: cylinders (SC2 and MC2), triangular bars (ST2 and MT2) and square bars (SS2 and MS2), respectively.

ignition, the flame front reached the front of the obstacles. After impinging on the obstacle, the flame front emerged from the large gap between the obstacle and the chamber side walls causing a series of vortex pairs around the obstacle. With increasing time, the flame starts to roll up behind the obstacle.

As indicated in Table 2, flame reconnection in the wake of the obstacle for all the configurations used occurred at about 60-88 ms after ignition. The fastest flame reconnection for single and multiple obstacles occurred with the square bars. While the slowest flame reconnection occurred with the cylinders. Note that the faster flame reconnection occurs with the lower blockage ratios rather than the higher blockage ratios, and for the single obstacles rather than the multiple ones for a given shape. After flame reconnection, the travel time of the propagating flame front to the chamber exit was around 72-86 ms after ignition for all the obstacles used.

The delay time of the flame exiting the chamber was shorter with the square obstacles, while the longest times occurred

Table 2. The flame reconnection times behind obstacle and delay times of the flame exiting the chamber after ignition for all the configurations.

| Symbol | Flame reconnection time (ms) | The delay time of the flame exiting the chamber (ms) |
|---|---|---|
| SC1 | 64 | 86 |
| SC2 | 82 | 78 |
| ST1 | 60 | 82 |
| ST2 | 78 | 78 |
| SS1 | 60 | 80 |
| SS2 | 72 | 72 |
| MC1 | 68 | 82 |
| MC2 | 88 | 78 |
| MT1 | 64 | 80 |
| MT2 | 82 | 76 |
| MS1 | 62 | 78 |
| MS2 | 78 | 72 |

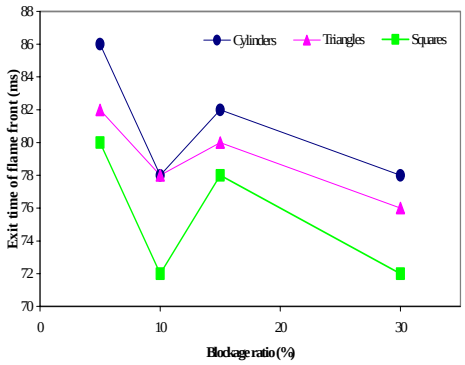


Fig. 3. Exit times for of the flame front as a function of blockage ratio.

with the cylinders. Fig. 3 shows the effects of increasing blockage ratio on the exit time of propagating flame front. The blockage ratio with 5 & 10% represent different single obstacles, and the 15 & 30 % are different multiple obstacles.

Unlike flame reconnection, the time taken to approach the chamber exit was found to be faster with the higher blockage ratios within obstacles of the same shape. This indicates that the flame acceleration behind the obstacle wake is proportional to the obstruction ratio.

Like the studies by Masri et al. [12], the time for the propagating flame to reach the chamber exit was shortest with the square obstacle for both the single and multiple obstacles, however, the fastest flame reconnection time behind the obstacle was found to be with the square obstacles in this study rather than the cylinder in the Masri.

As the flame front reached the chamber exit, the propagating flame front was moved laterally along the vent with an increase in flame surface area, pushing unburnt mixture ahead of it and air outside the chamber entered at the side of the vent away from the flame front. The interaction of flame around the obstacle with the vent caused complex vortices to form as flame spread along the obstacle towards the side of the chamber.

### 3.2 Effects on flame height and width

Fig. 4 shows the variations of flame height and width of the propagating flame front for all the obstacles at different times after ignition. The flame height was measured as the tip of the flame front above the base of the chamber until the flame front exited the chamber. The flame width was measured as the lateral width of the flame at the base of the chamber.

The longest flame height and width with the different single obstacles of 5 and 10% blockage ratio were obtained with the square bars being 252 and 403 mm (SS1), and 310 and 466 mm (SS2), respectively at about 74ms after ignition. The shortest flame height and width with 5 and 10% blockage ratio occurred with the cylinder being 211 and 381 mm (SC1), and 219 and 405 mm (SC2), respectively at about 74ms.

It was also clear that the flame height and width were longer with the multiple square obstacles with 15 and 30% obstruction ratio, being 246 and 419 mm (MS1), and 283 and 488 mm (MS2), respectively at about 74 ms. The multiple cylinder obstacles with 15 and 30% obstruction ratio were the shortest flame height and width, being 206 and 379 mm (MC1), and 208 and 436 mm (MC2), respectively at about 74 ms.

As shown in Fig. 5, as the obstruction ratio within obstacles of the same shape increased, the flame height also increased, and the increase with single obstacles was found to be higher than with multiple obstacles.

Although the acceleration of the flame front is similar to that obtained from small scale explosion tests by Masri et al. [12], the volume of unburnt mixture around the obstacle in this chamber which has very small L/D ratios of 0.235 and large rectangular top-venting, is in a different order.

After the flame reached the vent, the unreacted gas to the side of the chamber was pushed by the lateral flame spread through the vent. This resulted in faster lateral flame

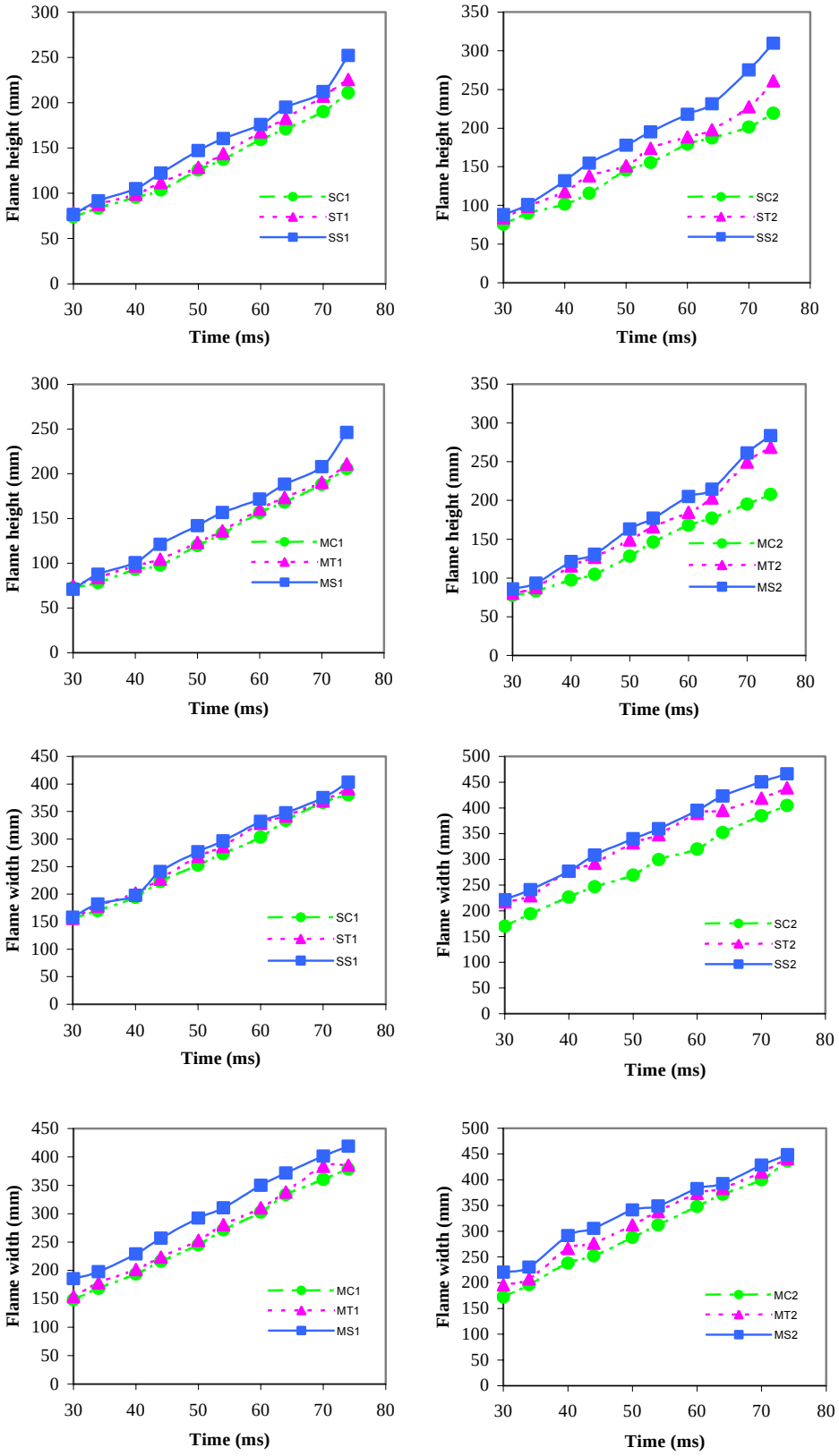


Fig. 4. Flame height and width with time after ignition for all the single and multiple obstacles used.

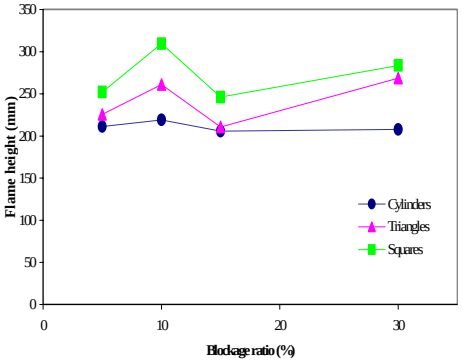


Fig. 5. Flame height against blockage ratio at 74ms after ignition for all the obstacles.

spread on top of the vent than within the chamber due to turbulent formation at the vent and hence higher flame speed compared to the internal environment.

As the square obstacle had the fastest development of flame height and width, lower amounts of unburnt gas exists within the chamber at any given time while the cylinders with the slower flame development caused higher volumes. The volume of unburnt mixture within the chamber decreased as obstruction ratio increased.

### 3.3 Effects on explosion pressure

Fig. 6 shows the influences of the different single and multiple obstacles on explosion pressure.

Cylinder obstacles with 5 % and 10% blockage ratio caused the highest overpressures: 75 mbar (SC1) and 57 mbar (SC2) occurred at 235 ms (SC1) and 210 ms (SC2), respectively. However, the square bars resulted in the lowest overpressure, with corresponding pressures of 49 mbar (SS1) and 25 mbar (SS2) at 201 ms (SS1) and 168 ms (SS2), respectively.

The highest overpressures with 15 and 30 % blockage ratio were also obtained with the cylinder obstructions. The peak pressure was 78 mbar at 244 ms (MC1), and 61 mbar at 226 ms (MC2). Again, the lowest

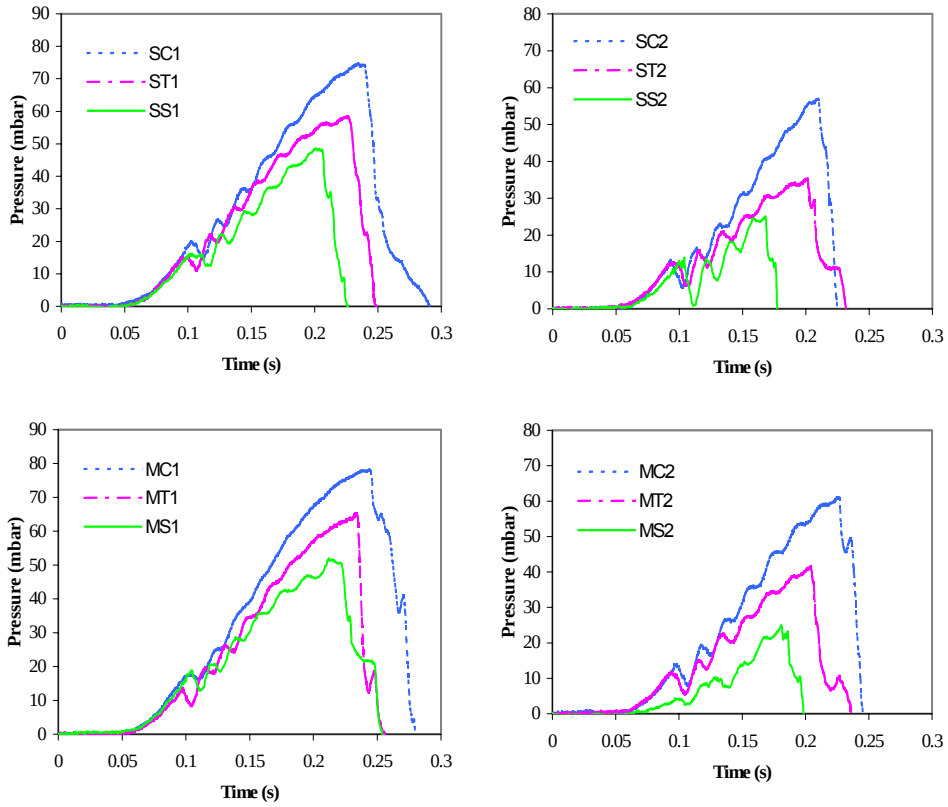


Fig. 6. Comparison of pressure-time history for the different single and multiple obstacles covering blockage ratio ranging from 5 % to 30%.

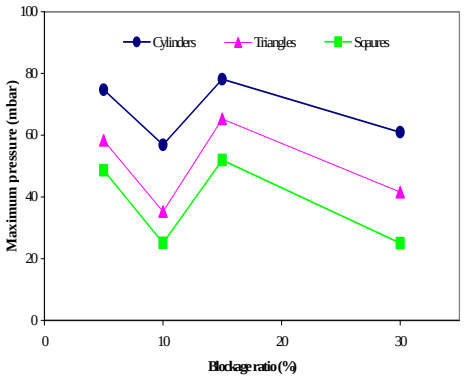


Fig. 7. Maximum pressure against blockage ratio for all the obstacles.

overpressures were obtained with the square obstructions, and the resulting maximum pressure was 52 mbar at 212 ms (MS1), and 25 mbar at 181 ms (MS2), respectively.

The time taken to reach the maximum pressure was found to be shorter with the square obstacle than the cylindrical obstacle, and decreased as the obstruction ratio increased for a given obstacle configuration. The pressure increases as the number of obstacles of a given width is increased but this change is less significant.

As shown in Fig. 7, as the obstruction ratio within the obstacles of the same shapes was increased, the explosion pressure decreased, and the pressure generated with single obstacles was lower than with multiple obstacles.

As discussed in the previous sections, the faster increase in the flame height and width may have caused the expulsion of a larger amount of the unburnt mixture within the chamber to the vent as well as increasing the inflow of air to the chamber. The net result is a decrease in the flame surface area and lower combustion rate and hence a lower pressure and shorter delay time taken to reach the peak pressure. The pressure development was constant for a given blockage ratio until about 100 ms in all experiments after which the pressure diverged.

Although the influence of the level of turbulence on the explosion pressure for different solid obstructions can clearly be seen enhancing flame acceleration in the same way as studies by Ibrahim and Masri [8], the results obtained in this study for similar objects were different due to the different configuration of the chamber used.

### 3.4 Effects on maximum rate of pressure rise & impulse to maximum pressure

Table 3 shows the results of the maximum rate of pressure rise and impulse to peak overpressures for all the obstacles.

The measurement for the maximum rate of pressure rise was performed by measuring the average slope through the pressure oscillations prior to the maximum pressure as shown in Fig. 6. The impulse was measured by integrating the pressure curve to maximum pressure.

As shown in Fig. 8, the effects on the rates of pressure rise and impulse against blockage ratio has a similar trend to explosion pressure as discussed in the previous section. The highest rate of pressure rise occurred with multiple cylinders (MC1) with a 15% blockage ratio while the lowest occurred the single square obstacle (SS2) with the 10% obstruction. Similarly the largest impulse occurred with multiple cylinders (MC1) due to the highest volume of the unreacted gas within the

Table 3. The maximum rates of pressure rise and impulses to the maximum peak pressure for the different single and multiple obstacles.

| Symbol | Maximum rate of pressure rise (mbar/s) | Impulse to maximum explosion pressure (mbar·s) |
|---|---|---|
| SC1 | 544 | 6.639 |
| SC2 | 477 | 3.850 |
| ST1 | 470 | 5.217 |
| ST2 | 301 | 2.612 |
| SS1 | 389 | 3.280 |
| SS2 | 286 | 1.178 |
| MC1 | 563 | 7.558 |
| MC2 | 482 | 4.914 |
| MT1 | 478 | 5.179 |
| MT2 | 338 | 2.897 |
| MS1 | 397 | 3.984 |
| MS2 | 321 | 1.012 |

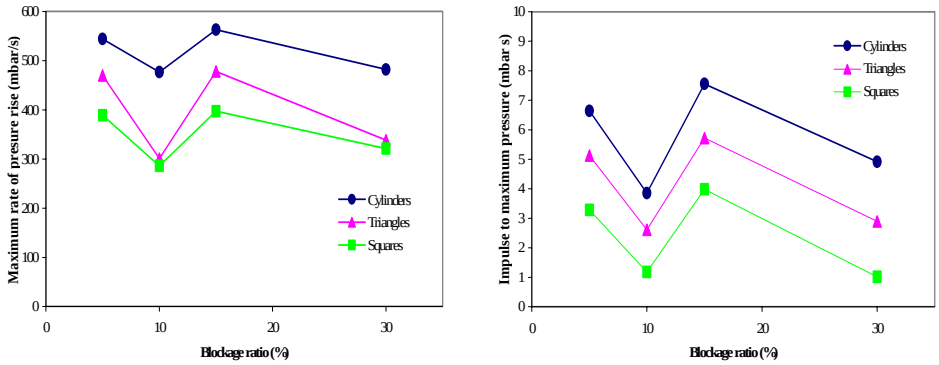


Fig. 8. The maximum rates of pressure rise and impulses to the max. pressure against blockage ratio for all the obstacles.

chamber while the smallest was obtained with the single square obstacle (SS2) due to the lowest volume of the unreacted gas within the chamber.

## 4. Conclusions

Experimental studies have been carried out to investigate the influence of different single and multiple shape obstructions in volumes will a small L/D ratio and large rectangular vent. Three different single and multiple obstacles with cylindrical, triangular and square cross-sections covering blockage ratios from to 5 to 30 % were used. The main results obtained from the present work are presented as follows.

1. The early flame propagation for all the obstacles used was an expanding hemisphere from the ignition point. The flame front emerging from the large gap between the obstacle and the chamber side walls caused flow vortices around the obstacle.

2. The fastest flame reconnection occurred with the square obstacles while the slowest was with the circular ones. Lower blockage ratio within the same obstacle configurations caused flame reconnection to be faster. Cylindrical obstructions produced the longest travel time for the flame exiting the chamber while the shortest occurred with square ones. Increasing obstruction ratios with the same obstacles were found to be faster.

3. The longest flame height and width were obtained with the square geometries while the shortest were observed with the circular ones. Also, increasing lengths occurred with increasing blockage ratio and with the single obstacles more than the multiple ones.

4. The cylinder type obstacles caused the highest overpressures due to the highest volume of the unburnt mixture around the obstacles while the lowest was obtained with the square obstacles due to the lowest volume of the unburnt gas. As the obstruction ratio was increased, the explosion pressure decreased, and the pressure in the single obstacles was lower than with the multiple obstacles. The rate of pressure rise and impulse were shown to be a similar trend to the explosion pressure.

## Acknowledgements

The authors gratefully acknowledge for the financial support by R&D Training Centre, Korea Gas Corporation.

## References


1. Bakke J.R. and Hjertager B.H., “The effect of explosion venting vessels”, International J. for Numerical Methods in Engineering, Vol. 24, pp.129-140 (1987).
2. Bjerketvedt, D., Bakke, J.R. & Van wingerden, K., “Gas Explosion Handbook”, J. Hazardous Materials, Vol. 52, pp. 1-150 (1997).
3. Fairweather M., Hargrave G.K, Ibrahim S.S and Walker D.G., “Studies of Premixed Flame Propagation in Explosion Tubes”, Combust. Flame, 116: pp. 504-518 (1999).
4. Green, A.R. & Nehzat, N., “Experimental studies of flame propagation and pressure rise in a 1:54 scale coal mine model”, Australian Symp. on Combustion and The Sixth Australian Flame Days, pp. 170-174 August, (1999).
5. Hjertager, B.H., “Computer modeling of turbulent gas explosions in complex 2D and 3D geometries”, J. of Hazardous Materials, Vol. 34, pp. 173-197 (1993).
6. Hjertager, B.H., Fuhre, K., & Bjorkhaug, M., “Concentration Effects on Flame Acceleration by Obstacles in Large-Scale Methane-Air and Propane-Air Vented Explosions”, Combust. Sci. Tech., Vol. 62, pp. 239-256 (1988).
7. Ibrahim, S.S., Hargrave, G.K., & Williams, T.C., “Experimental investigation of flame/solid interactions in turbulent premixed combustion”, Experimental Thermal & Fluid Science, Vol. 24, pp. 99-106 (2001).
8. Ibrahim, S.S. & Masri, A.R., “The effects of obstructions on overpressure resulting from premixed flame deflagration”, J. Loss Prev. in the Process Ind., No. 14, pp. 213-221 (2001).
9. Khan, F.I. & Abbasi, S.A., “Major accidents in process industries and an analysis of causes and consequences”, J. Loss Prev. in the Process Ind., No. 12, pp. 361-378 (1999).
10. Koshy, A. Mallikarjunan, M.M and Raghavan, K.V., “Causative factors for vapour cloud explosions determined from past-accident analysis”, J. Loss Prev. in the Process Ind., Vol. 8, No. 6, pp. 355-358 (1995).
11. Lenoir, E.M. & Davenport, J.A., “A Survey of Vapor Cloud Explosions: Second Update”, Process Safety Progress, Vol.12, No. 1, pp. 12-33 (1993).
12. Masri, A.R., Ibrahim, S.S., Nehzat, N., & Green, A.R., “Experimental study of premixed flame propagation over various solid obstructions”, Experimental Thermal and Fluid Science, Vol. 21, pp. 109-116 (2000).
13. Moen, I.O., Donato, M., Knystautas, R. & Lee, J.H., “Flame Acceleration Due to Turbulence Produced by Obstacles”, Combust. Flame, Vol. 39, pp. 21-32 (1980).
14. Moen I.O. and Lee J.H.S., “Pressure Development Due to Turbulent Flame Propagation in Large-Scale Methane-Air Explosions”, Combust. flame, 47, pp. 31-52 (1982).
15. Phylaktou, H., & Andrews, G.E., “Gas Explosions in Long Closed Vessels”, Combust. Sci. and Tech., Vol. 77, pp. 27-39 (1991).
16. Popat N.R., Catlin C.A., Arntzen B.J., Lindstedt R.P., Hjertager B.H., Solberg T., Saeter O., Van den Berg A.C., “Investigations to improve and assess the accuracy of computational fluid dynamics based explosion models”, J. of Hazardous Materials, vol. 45, pp. 1-25 (1996).
17. Pritchard D.K., Freeman D.J. and Guilbert P.W., “Prediction of explosion pressures in confined spaces”, J. Loss Prev. Process Ind., Vol. 9. No.3, pp. 205-215 (1996).
18. Urtiew P.A., Brandeis J. and Hogan W.J., “Experimental Study of Flame Propagation in Semiconfined Geometries with Obstacles”, Combust. Sci. Tech., Vol. 30, pp. 105-119 (1983).
19. Starke R. and Roth P., “An Experimental Investigation of Flame Behavior During Explosions in Cylindrical Enclosures with Obstacles”, Combust. flame, 75, pp. 111-121 (1989).